9 January 2026

An integrative biophysical and computational workflow uncovers new allosteric sites and modulators of the human A2A adenosine receptor

Renaud Prudent[4], Arka Ray[1], Naveen Thakur[1], Alexis Moreno[5], Tana Tandaric[6,2], Hugues Lemoine[4], Elsa Forcellini[4], Erika Cecon[7], Didier Roche[4], Ralf Jockers[7], Hugo Gutiérrez de Terán[2,3], Matthew Eddy[1]

1. Department of Chemistry; University of Florida; Gainesville, FL, 32611; USA

2. Ruđer Bošković Institute, Zagreb, Croatia

3. Nanomaterials and Nanotechnology Research Center (CINN), Spanish National Research Council (CSIC), Health Research Institute of Asturias (ISPA), 33011 Oviedo, Asturias, Spain

4. Edelris, Bioparc, Bioserra 1 building, Lyon ; France

5. Eurofins Calixar, Laennec building, Lyon ; France

6. Department of Cell and Molecular Biology, Uppsala University, Sweden

7. Université Paris Cité, Institut Cochin, INSERM, CNRS, 75014 Paris, France

Abstract

Allosteric modulators offers a promising approach for targeting receptor function in pathological contexts. Although numerous orthosteric ligands have been developed, the discovery of allosteric inhibitors remains limited, hindered by challenges with identifying modulators and the perceived lower druggability of allosteric sites. In this study, we employed affinity selection–mass spectrometry (AS-MS) with a chemically diverse library to identify novel allosteric modulators of the human A2A adenosine receptor (A2AAR). Subsequent competition binding and orthogonal biophysical assays confirmed the allosteric nature of multiple initial hits, underscoring the sensitivity and utility of the AS-MS approach. Despite exhibiting relatively weak affinity at the orthosteric binding site, these compounds modulated cAMP production, supporting the idea that allosteric modulators can exert functional effects without requiring high potency to outcompete endogenous adenosine. Experiments in the presence an A2AAR agonist further supported the classification of these compounds as negative allosteric modulators (NAMs), with distinct pharmacological profiles indicative of diverse mechanisms of action. An integrated computational workflow designed to predict allosteric sites and model ligand interactions provided insight into potential binding poses, yielding both intracellular and extracellular allosteric sites that

aligned with the experimentally observed pharmacological properties. The identification of these previously uncharacterized NAMs represents an important step toward developing alternative A2AAR-targeted therapies, enabling pharmacological intervention through receptor sites beyond the orthosteric binding pocket.

Keywords

GPCR, A2A Adenosine Receptor, Allosteric Modulators, Drug Discovery

An integrative biophysical and computational workflow uncovers new allosteric sites and modulators of the human A_{2A} adenosine receptor

Renaud Prudent[1,*], Arka P. Ray[2], Naveen Thakur[2], Alexis Moreno[3], Tana Tandaric[4,5], Hugues Lemoine[1], Elsa Forcellini[1], Erika Cecon[6], Didier Roche[1], Ralf Jockers[6], Hugo Gutiérrez de Terán[5,7,*], Matthew T. Eddy[2,*]

[1]Edelris, Bioparc, Bioserra 1 building, Lyon ; France

[2]Department of Chemistry; University of Florida; Gainesville, FL, 32611; USA

[3]Eurofins Calixar, Laennec building, Lyon ; France

[4]Department of Cell and Molecular Biology, Uppsala University, Sweden

[5] Ruđer Bošković Institute, Zagreb, Croatia

[6]Université Paris Cité, Institut Cochin, INSERM, CNRS, 75014 Paris, France

[7]Nanomaterials and Nanotechnology Research Center (CINN), Spanish National Research Council (CSIC), Health Research Institute of Asturias (ISPA), 33011 Oviedo, Asturias, Spain

*Corresponding authors: Renaud Prudent (renaud.prudent@edelris.com); Hugo Gutiérrez de Terán (h.g.teran@cinn.es); Matthew T. Eddy (matthew.eddy@ufl.edu)

ABSTRACT

Allosteric modulators offers a promising approach for targeting receptor function in pathological contexts. Although numerous orthosteric ligands have been developed, the discovery of allosteric inhibitors remains limited, hindered by challenges with identifying modulators and the perceived lower druggability of allosteric sites. In this study, we employed affinity selection–mass spectrometry (AS-MS) with a chemically diverse library to identify novel allosteric modulators of the human A_{2A} adenosine receptor (A_{2A}AR). Subsequent competition binding and orthogonal biophysical assays confirmed the allosteric nature of multiple initial hits, underscoring the sensitivity and utility of the AS-MS approach. Despite exhibiting relatively weak affinity at the orthosteric binding site, these compounds modulated cAMP production, supporting the idea that allosteric modulators can exert functional effects without requiring high potency to outcompete endogenous adenosine. Experiments in the presence an A_{2A}AR agonist further supported the classification of these compounds as negative allosteric modulators (NAMs), with distinct pharmacological profiles indicative of diverse mechanisms of action. An integrated computational workflow designed to predict allosteric sites and model ligand interactions provided insight into potential binding poses, yielding both intracellular and extracellular allosteric sites that aligned with the experimentally observed pharmacological properties. The identification of these previously uncharacterized NAMs represents an important step toward developing alternative A_{2A}AR-targeted therapies, enabling pharmacological intervention through receptor sites beyond the orthosteric binding pocket.

INTRODUCTION

The human A_{2A} adenosine receptor (A_{2A}AR) is a class A G protein-coupled receptor (GPCR) that plays a critical immunosuppressive role in the tumor microenvironment by dampening the activity of effector T cells and natural killer (NK) cells, thereby promoting tumor immune evasion.[1-3] Beyond oncology, A_{2A}AR is implicated in a range of pathological conditions, including neurodegenerative and inflammatory diseases, where its modulation influences both immune and neuronal signaling pathways.[4-6] A_{2A}AR antagonists therefore have emerged as valuable molecular tools and therapeutic candidates, with relevance to neurological disorders and cancer immunotherapy. While early clinical efforts in Parkinson's disease were limited by efficacy and safety concerns, multiple A_{2A}AR antagonists have progress in oncology and remain under evaluation for the treatment of solid tumors.[1] Dysregulation of the adenosine signaling axis contributes to resistance against PD-1/PD-L1 checkpoint inhibitors, positioning A_{2A}AR as an attractive target for enhancing immunotherapeutic responses.[2,3,6] However, compensatory upregulation of CD73 can elevate extracellular adenosine within the tumor microenvironment,[4] potentially diminishing the effectiveness of orthosteric A_{2A}AR blockade. This challenge has motivated the development of bifunctional compounds capable of simultaneously targeting CD73 and A_{2A}AR.[5]

Allosteric modulation represents an alternative therapeutic strategy with the potential to finely tune A_{2A}AR activity and circumvent adaptive resistance mechanisms. Amiloride and related derivatives have been reported as negative allosteric modulators (NAMs) of A_{2A}AR,[7] thought to act through the highly conserved sodium ion pocket characteristic of many class A GPCRs.[8] Among these, hexamethylene amiloride (HMA) exhibits relatively potent NAM activity with low-micromolar binding affinity, yet it lacks receptor selectivity and remains primarily a pharmacological probe rather than a viable therapeutic lead. These limitations underscore the need to identify more selective and tractable A_{2A}AR allosteric modulators.

Affinity selection–mass spectrometry (AS-MS) has emerged as a powerful ligand discovery platform for complex targets, including GPCRs,[9] with the potential to discover allosteric modulators. Prior studies have applied AS-MS to identify small-molecule allosteric modulators of A_{2A}AR that engage the sodium pocket, including an

investigational compound with reported activity of IC_{50} ~15 μM.[9] However, these initial leads have not yet been advanced toward therapeutic optimization. Here, we employed an AS-MS–based workflow to discover novel allosteric modulators of A_{2A}AR, leveraging Keymical Space™, a large structurally-diverse compound library based on three-dimensional structural mimetics of natural product chemotypes. We predicted that this chemical diversity could increase the likelihood of identifying ligands capable of engaging previously uncharacterized allosteric sites. A key advantage of our AS-MS based strategy is the ability to perform screening using the native, full-length receptor[10] without requiring stabilizing mutations or specialized detergents, thereby preserving physiologically relevant receptor conformations. Through this approach, we identified several hit compounds that interacted with A_{2A}AR. Comprehensive biophysical and pharmacological characterization, including competition binding, cAMP signaling assays, and orthogonal biophysical measurements, indicated that these molecules function as candidate allosteric modulators acting outside the orthosteric binding pocket.

To obtain further structural insight into how the newly identified compounds modulated A_{2A}AR activity, we herein present a novel integrative computational workflow to predict potential allosteric binding sites and explore ligand binding orientations within these regions. Our workflow accounts for the multiple potential thermodynamic mechanisms by which allosteric modulators can affect GPCR activity. Predominantly enthalpic effect reflects changes in the average receptor conformation, whereas entropic effects primarily influence fluctuations around a mean conformation.[11,12] In most cases, however, modulator binding perturbs the allosteric communication network that connects the orthosteric binding pocket to intracellular effector-binding surfaces, modulating internal motions, i.e., confirmational entropy, within the receptor or receptor signaling complex.[13] The workflow developed for this study accounts for both large-scale changes in the conformational equilibrium between active and inactive states, and local fluctuations within each state, by independent molecular dynamics sampling of both active and inactive receptor conformations. Our approach identified both extracellular and intracellular allosteric sites, with predicted binding modes that aligned with the experimentally observed biophysical and pharmacological properties of the compounds. Together, these findings highlight both new chemical matter and new mechanistic

possibilities for A_{2A}AR allosteric modulation. The implications of these results for future efforts to develop selective A_{2A}AR allosteric modulators are discussed.

RESULTS

AS-MS screening of A_{2A}AR ligands

Affinity Selection–Mass Spectrometry (AS-MS) screening was performed with the full-length native human A_{2A}AR obtained from previously published protocols developed at Eurofins Calixar.[14] We began by comparing the two widely utilized methods based on size exclusion chromatography–mass spectrometry (SEC-MS) for hit identification, the 2D-liquid chromatography (LC)–based Automated Ligand Identification System (ALIS)[15] and microplate-based SpeedScreen.[16] The microtiter plate method provided superior results, based on observed higher signal intensities and improved signal-to-noise ratios (Figure 1A). Saturation of the mass signal of the antagonist ZM241385 was obtained with higher intensity with the SpeedScreen method at 3.3 µM A_{2A}AR compared to ALIS (Figure 1A).

A_{2A}AR was screened against 300,000 compounds plated in pools of 500 compounds each. Screening was performed at 3.3µM A_{2A}AR and 1µM of each compound. Hit potencies were evaluated based on their binding ratio (defined as the ratio of MS signal of a compound, as [M+H]+ ion, from post-SEC sample containing A_{2A}AR minus the corresponding signal from post-SEC sample without A_{2A}AR (background), divided by signal from sample pre-SEC (without A_{2A}AR to spare protein amount), (Figure 1B).

From the initial set of compounds, 8,367 compounds were obtained as primary hits (primary hit rate of 2.8%). Because this initial hit rate was unexpectedly high, we hypothesized that some of the potential hits were due to non-specific interactions, including hydrophobic interactions. We therefore removed any potential hits that were also identified as ligands for bovine serum albumin (BSA). Following this, a structural filter was applied to remove potential aggregators and favor chemical diversity through clustering analysis.[17] 98 selected hits were then confirmed in a second round of SEC-MS assays in the presence of 10 µM ZM241385. This secondary screening led to the confirmation of 37 hits (37.7% secondary hit rate). Hits were resynthesized and assayed at a single concentration. The best hits were then submitted to concentration-response experiments leading to 19 confirmed compounds.

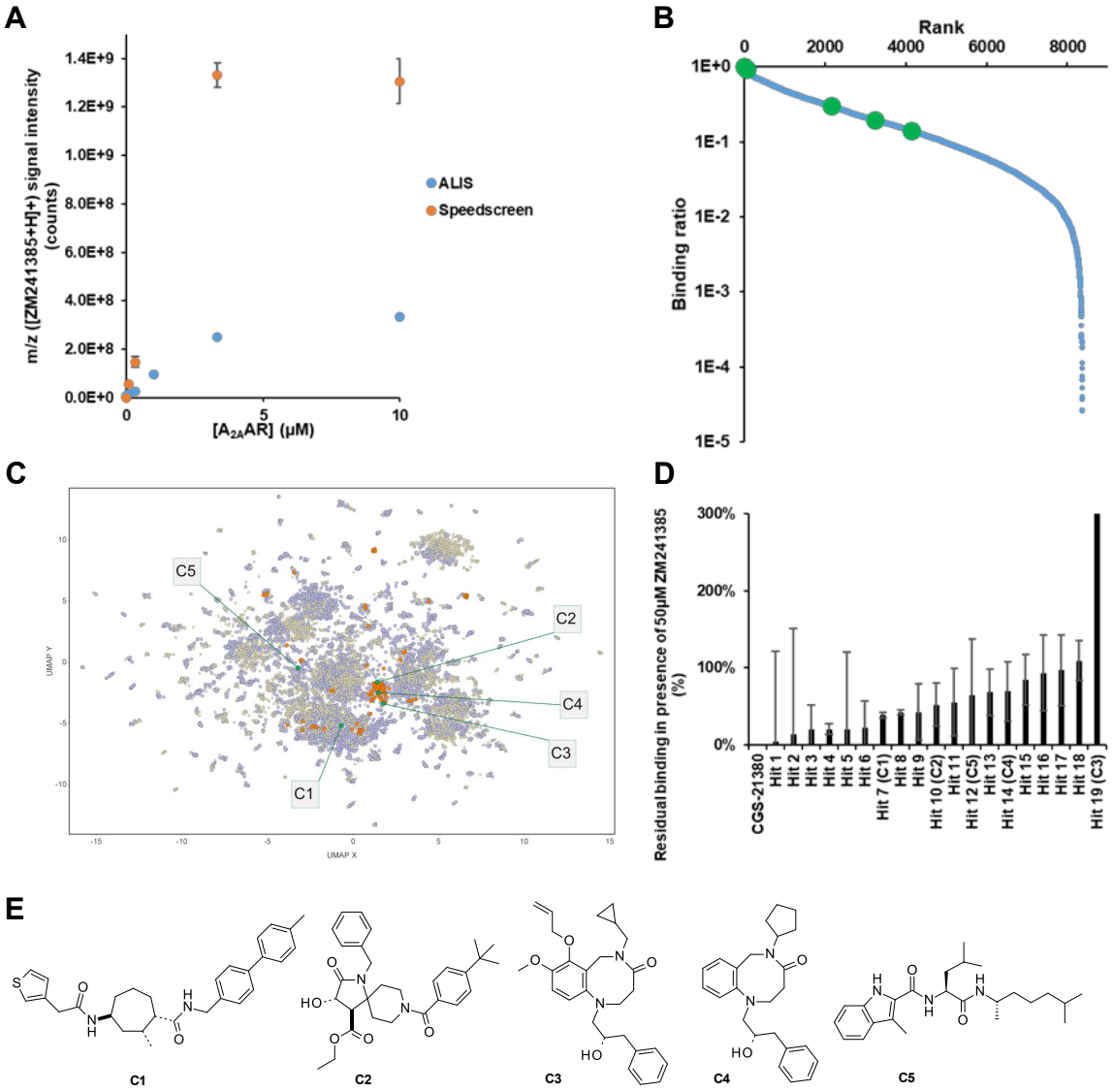

Figure 1. Identification of $A_{2A}AR$ allosteric hits by SEC-MS. (A) SEC-MS methods comparison using ZM241385 as a benchmark compound. The post-SEC reference compound ZM241385 MS signal is plotted against $A_{2A}AR$ concentration. Saturation of the mass signal of ZM241385 is obtained at 3 μM $A_{2A}AR$ for both methods but the signal is almost 10 times higher with the plate-based method. Post-SEC MS signals from the ALIS offline method (blue dots) or from the plate-based method (orange dots) are shown. (B) Ranking of primary hits based on binding ratio (BR). Compounds with BR >0.01 were considered for evaluation in secondary screening. Compounds characterized later in this study are highlighted as green circles (binding ratio for C1: 0.93 ; C2: 0.14 ; C3: 0.30 ; C4: 0.20 ; C5: 1.06). (C) AS-MS hits clustering; UMAP visualization of the 8367 hits using the SkeletonSpheres descriptor[14], colored by categories of hits. Hits from primary screening (pale violet) are disseminated around several clusters, whereas hits from secondary screening (orange) are centered on specific areas of the map. Non-specific ligands (beige) were removed from the selection for secondary screening. The best hits confirmed with orthogonal methods are colored in green and labeled C1 through C5. Compounds C2, C3, and C4 belong to a cluster with several hits confirmed in the secondary screening. Compounds C1 and C5 belong to different clusters. (D) SEC-MS competition assay between ZM241385 and confirmed hits. Orthosteric $A_{2A}AR$ agonist CGS-21380 was used as a control (1μM) and was fully displaced with 50μM ZM241385. (E) Chemical structures of compounds C1 through C5 identified in the AS-MS screening campaign and further studied.

AS-MS assays for allosteric ligand identification

To rule out potential interference from other compounds present in the pools containing the hits of interest, another round of SEC-MS–based competition assays were performed on single compounds using an excess of ZM241385 (50 μM) to saturate the A_{2A}AR orthosteric binding pocket and 1 μM of each hit compound. With this workflow, we aimed to assess whether any observed compounds interacted with A_{2A}AR at locations that did not directly overlap with the ZM241385 binding site in the A_{2A}AR orthosteric pocket. CGS-21680 was used as a control orthosteric A_{2A}AR agonist. In the presence of 50 μM ZM241385, CGS-21680 was no longer detected in the post-SEC fraction containing A_{2A}AR, indicating that it was displaced from the orthosteric site due to competitive binding. In contrast, several hit compounds co-eluted with A_{2A}AR in the presence of a saturating concentration of ZM241385, supporting the idea that these hits bind to non-overlapping, potentially allosteric sites on A_{2A}AR. Based on these results, a diverse panel of 5 hits was selected for further investigation (Fig. 1C), referred to as C1 (Hit 7), C2 (Hit 10), C3 (Hit 19), C4 (Hit 14) and C5 (Hit 12).

Characterization of ligand binding through a fluorescence thermal shift assay

Ligand binding to GPCRs can be assessed by monitoring shifts in the thermal stability of the receptor, typically observed as changes in the melting temperature (T_m) relative to the unliganded (apo) state. This phenomenon, referred to as a thermal shift, reflects ligand-induced stabilization of the receptor fold.[18] The largest increases in T_M values are typically observed for compounds that bind at orthosteric sites.[18] We therefore hypothesized that hits that were strictly allosteric binding compounds would exhibit no increases to only marginal increases in observed T_m values, whereas hits that may interact with orthosteric sites would exhibit larger increases in T_m values.

We employed a fluorescence-based thermal shift assay to assess the interaction of compounds C1 through C5 with purified human A_{2A}AR solubilized in DDM/CHS mixed micelles. Thermal denaturation was monitored using the thiol-reactive fluorescent dye 7-diethylamino-3-(4′-maleimidylphenyl)-4-methylcoumarin (CPM), which selectively reacts with cysteine residues that become solvent-accessible upon protein unfolding.[18] All samples exhibited sigmoidal thermal unfolding profiles, indicative of well-folded receptor

preparations (Figure 2). Compounds C2, C3, and C5 exhibited melting curves with T_m values comparable to that of the apo receptor, suggesting minimal effect on receptor stability (Figure 2 and Table S1). For compound C1, we observed an increase in the melting temperature with respect to the apo receptor of approximately 2 ºC, comparable to the observed increase in T_m for the known A_{2A}AR antagonist caffeine (Figure 2 and Table S1), suggesting an increase in the thermal stability of the receptor due to interaction with compound C1, while compound C4, induced a decrease in the measured T_m of the receptor. The marginal changes observed for the receptor's T_m in the presence of compounds C2, C3 and C5 suggested that they did not form strong non-covalent interactions with the A_{2A}AR orthosteric binding pocket, consistent with the idea that these compounds could be interacting with the receptor at locations outside of the orthosteric pocket. In contrast, the increase in T_m for compound C1 indicated that this compound at least partially interacted with the A_{2A}AR orthosteric binding pocket or interacted both with the orthosteric binding pocket and potentially at an additional allosteric site.

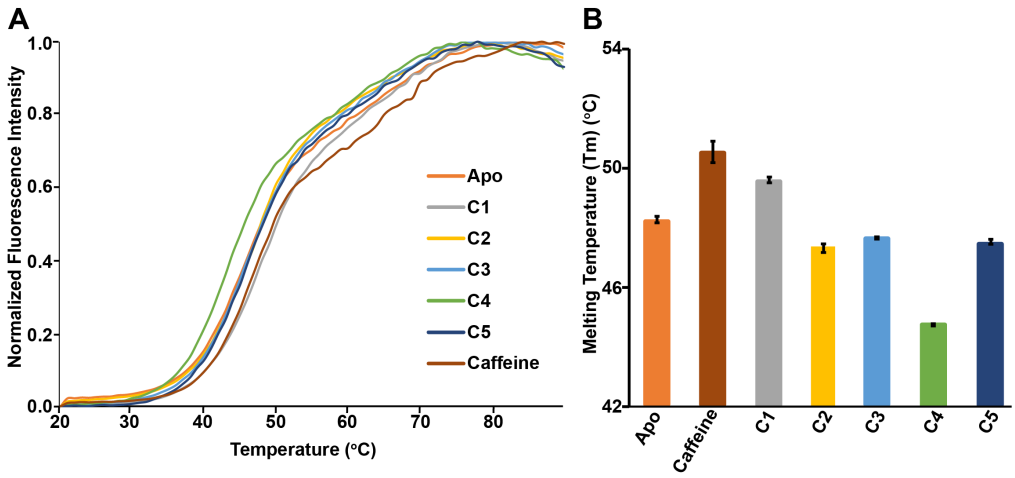

Figure 2. Characterization of A_{2A}AR interactions with ligands via a fluorescence thermal shift assay. (A) Fluorescence-observed thermal unfolding of human A_{2A}AR without ligand added (apo) and in the presence of caffeine or one of the five identified compounds, labeled 'C1' through 'C5'. (B) Thermal melting (T_m) values determined from the plots in A of A_{2A}AR without ligand added or in the presence of ligand. Error bars represent the s.e.m. from n ≥ 3 independent experiments. See also Table S1.

Characterization of ligand binding through a microscale thermophoresis spectral shift binding assay

We further characterized the direct binding of compounds C1-C5 to $A_{2A}AR$ by a spectral shift binding assay, also known as microscale thermophoresis (MST) (Figure 3). Purified $A_{2A}AR$ in DDM/CHS mixed micelles was labeled by a red-tris-NTA fluorescent probe and mixed with increasing concentrations of the selected compounds before measuring the fluorescence emissions at 670 nm and 650 nm. The spectral shift, expressed as the ratio of the fluorescence emission intensity 670 nm vs 650 nm, was plotted against the concentration of each compound to determine the dissociation constant using the K_D model equation derived from the law of mass action. Compound C2 exhibited the highest affinity for $A_{2A}AR$ with a K_D of 64 μM, followed by C1 (K_D = 67 μM) and C3 (K_D = 81 μM). C4 bound $A_{2A}AR$ with a K_D of 142 μM, however with a poor spectral shift signal/noise ratio and low confidence in the determined value (Figure 3E). Finally, C5 exhibited the lowest affinity to $A_{2A}AR$ with an estimated K_D in the millimolar range (Figure 3C).

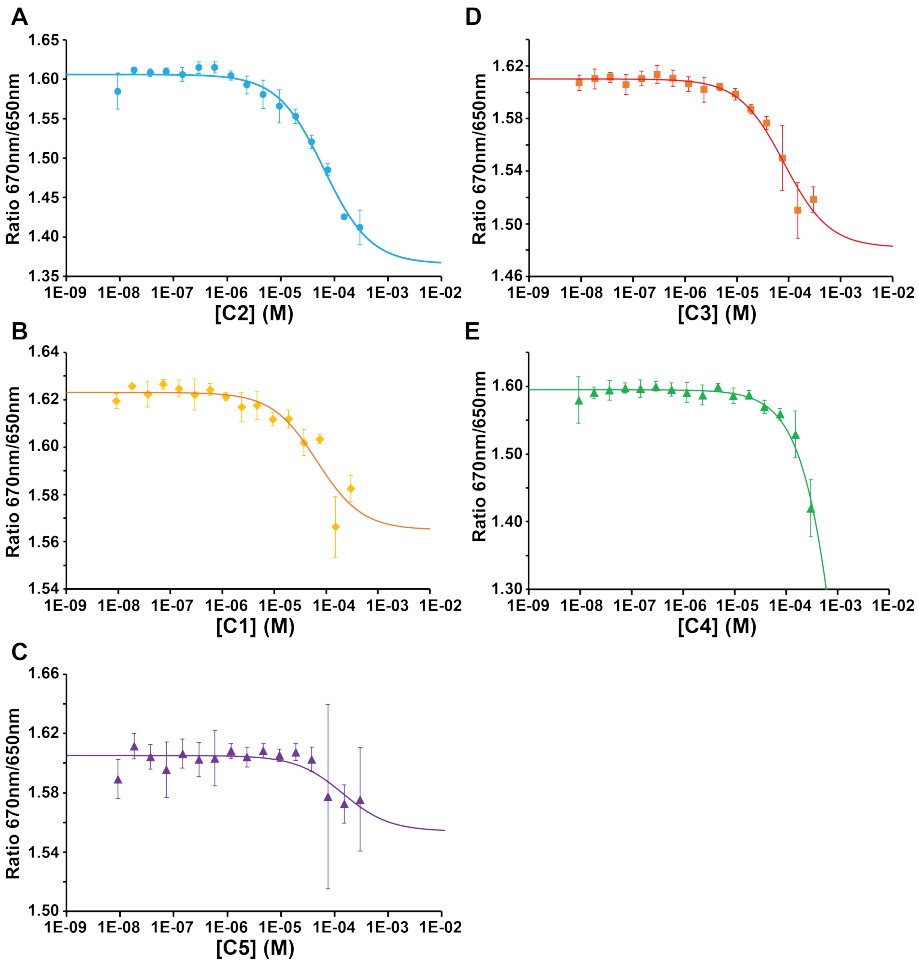

Figure 3. Binding of compounds to $A_{2A}AR$ measured by a thermophoresis spectral shift assay. (A-E) Fluorescence spectral shift, expressed as the ratio of fluorescence intensities measured at 670 nm and 650 nm, is plotted as a function of increasing concentration of each compound. Each assay utilized 50 nM of purified and labeled $A_{2A}AR$. Error bars represent the standard deviation from n = 3 independent experiments and two measurements per experiment. Data were fitted by non-linear regression using the K_D model equation.

Radioligand competition binding experiments with known orthosteric ligands

We further assessed the binding modes of compounds C1 through C5 with $A_{2A}AR$ and attempted to quantify their orthosteric binding affinities using a radioligand competition binding assay with the ^{3}H-labeled antagonist ZM241385. While MST experiments can be sensitive to binding of either allosteric or orthosteric ligands to the receptor, radioligand competition assays specifically test for ligand interactions with the receptor orthosteric pocket. Membrane fractions containing human $A_{2A}AR$ were prepared following established protocols.[19,20] In control experiments, we determined a K_D value of 7.4 ± 0.5

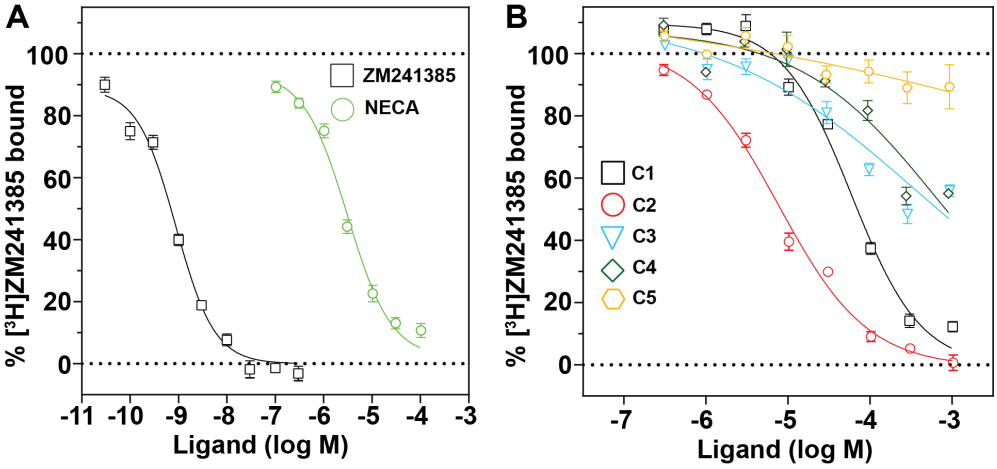

Figure 4. Radioligand competition binding assays. (A) Competition binding assays with the antagonist ZM241385 and full agonist NECA. The determined K_D value for ZM241385 was 7.4 ± 0.5 nM and the K_I value for NECA was 75.5 ± 2.8 nM. (B) Competition binding assays with compounds C1 through C5. The determined KI values were 65.6 ± 2.4 μM for C1, 285.9 ± 3.2 μM for C2, 241.6 ± 6.7 μM for C3, 348.4 ± 8.4 μM for C4, and > 1000 μM for C5. Error bars represent the s.e.m. from n ≥ 3 independent experiments. See also Table S2.

nM for the antagonist ZM241385 and a K_I value of 75.5 ± 2.8 nM for full agonist NECA (Fig. 4A and Table S2), in agreement with previously reported values for $A_{2A}AR$ expressed in insect cells.[21]

In heterologous competition binding experiments with compounds C1 through C5, compounds C1–C4 exhibited modest to weak binding affinities. Among them, compound C2 showed the highest affinity, with a measured K_D value of 65.6 ± 2.4 μM (Figure 4B and Table S2). This value closely agreed with the measured affinity of compound C2 from the MST assay (Figure 3) and supported the hypothesis that compound C2

interacted with the orthosteric binding pocket (see Discussion). This was in contrast to the observed affinities for C1 and C3, which were approximately a factor of 5 to 6 times weaker in the radioligand competition assays as compared with the MST assays, suggesting these compounds may interact with A2AAR primarily outside of its orthosteric binding pocket (see Discussion).

Radioligand binding assay testing potential allosteric interactions

To test our hypothesis that at least several of the hits were allosteric ligands, we performed two additional competition binding assays based on earlier reported experiments used to characterize the effects of amiloride-based NAMs[22]. In these assays, competition binding was measured in the absence and presence of a potential allosteric modulator. An allosteric effect is expected to manifest as an increase in apparent orthosteric affinity for a positive allosteric modulator (PAM) or a decrease for a negative allosteric modulator (NAM), relative to measurements made in the absence of the compound. We applied this approach to four ligands (C1–C4); C5 was excluded due to limited availability and very weak affinity in MST experiments (Figure 3). To conserve material, full dose–response curves were not collected. Instead, assays were performed at two concentrations of each compound. One set of experiments were recorded by incubating the receptor with the [^{3}H]-labeled antagonist ZM241385 and 1 μM unlabeled agonist NECA, while the second incubated the receptor with the [^{3}H]-labeled agonist CGS21680 and varying concentrations of unlabeled NECA.

In the first set of experiments, human A_{2A}AR in membrane fractions was incubated with 0.5 nM [^{3}H]-ZM241385 and 1 μM unlabeled NECA. For each condition, we added either 10 μM or 50 μM of compounds C1–C4 and measured the amount of remaining [^{3}H]-ZM241385. In the control condition with 1 μM NECA alone, 73.2% of [^{3}H]-ZM241385 remained bound (Figure 5 and Table S3). Upon addition of 10 μM of each compound, we observed a further decrease in the amount of radioligand remaining: 51.9% for C1, 65.1% for C4, 58.7% for C3, and 39.6% for C2 (Figure 5A and Table S3). Notably, compound C2 showed the largest reduction, suggesting a significant effect on NECA-mediated displacement.

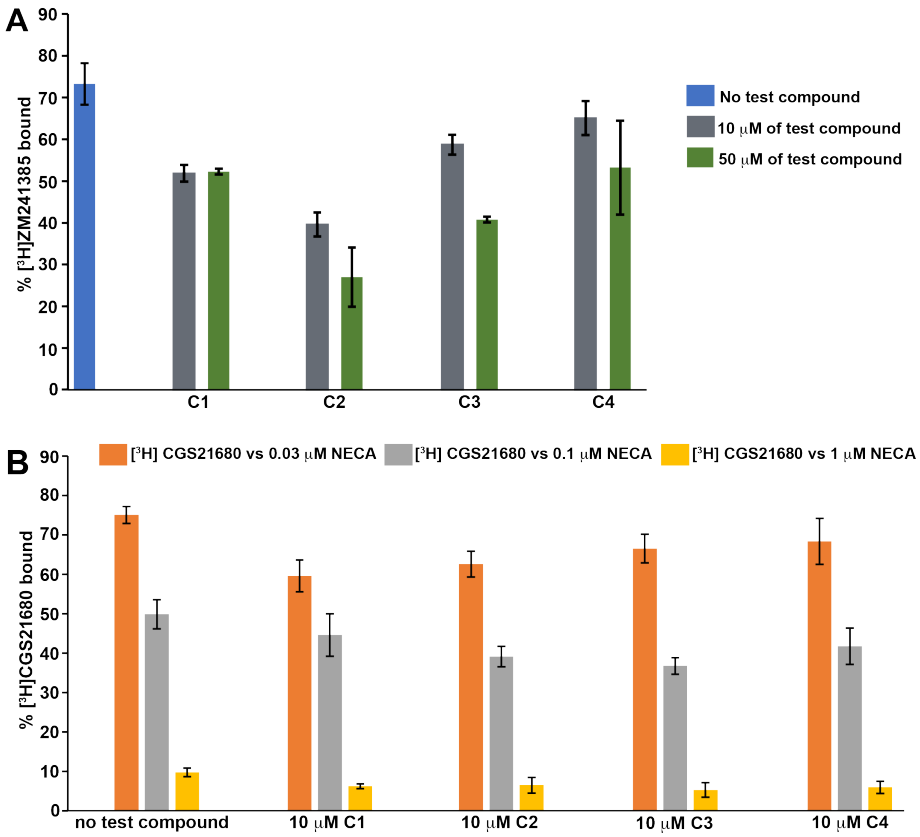

Figure 5. Radioligand competition experiments in the absence and presence of compounds C1 through C4. (A) Displacement of [^{3}H]-labeled antagonist ZM241385 with the agonist NECA in the absence and presence of 10 μM (grey bars) or 50 μM (green bars) of compounds C1 through C4. (B) Displacement of [^{3}H]-labeled agonist CGS21680 with NECA in the absence and presence of compounds 1 through 4. Error bars represent the s.e.m. from n ≥ 3 independent experiments. See also Tables S3 and S4.

To assess concentration dependence, a second series of assays was conducted using 50 μM of each compound. In these experiments, compound C1 produced no meaningful additional effect beyond what was observed at 10 μM (Figure 5A and Table S3). In contrast, compounds C2–C4 further reduced [^{3}H]-ZM241385 binding in a dose-dependent manner, with 27.0%, 40.1%, and 53.2% of the radioligand remaining for 50 μM of compounds C2, C3, and C4, respectively (Figure 5A and Table S3). The clear concentration-dependent effects of compounds C2 and C3 support their roles as potential negative allosteric modulators of A_{2A}AR, with compound C2 showing the most pronounced effect.

The above competition experiments were tested with A_{2A}AR in membranes incubated with the [^{3}H]-labeled antagonist ZM241385. To test whether we observed an impact of compounds C1–C4 on agonist binding, we incubated A_{2A}AR-containing membranes with 0.5 nM of the [^{3}H]-labeled full agonist CGS21680 and varying amounts of the unlabeled full agonist NECA in the presence of 10 μM of compounds C1–C4 (Figure 5B and Table S4). In the absence of compounds C1–C4, we observed a reduction in the fraction of bound [^{3}H]-CGS21680 to 75.1% in the presence of 0.03 μM NECA. Compared with this measurement, we observed a further reduction in the fraction of bound [^{3}H]-CGS21680 upon addition of the compounds C1–C4, to 68.4% for C4, 66.5% for C3, 62.6% for C2, and 59.6% for C1 (Figure 5B and Table S4). Additional reduction in the fraction of bound [^{3}H]-CGS21680 was observed in the presence of compounds C1–C4 for 0.1 μM and 1 μM NECA (Figure 5B and Table S4). Taken together, these data indicated that compounds C1–C4 acted as negative allosteric modulators for both orthosteric antagonists, or inverse agonists, and agonists. However, a larger impact was observed on orthosteric antagonists or inverse agonists for all compounds.

Assessing the impact of hit compounds on cAMP signaling in HEK293 cells

We next evaluated the effect of compounds C1-C5 on A_{2A}AR signaling by monitoring the effects of each compound on cAMP production in HEK293 cells. HEK293 cells stably expressing A_{2A}AR were incubated with each compound and cAMP production was quantified. The full agonist CGS-21680 and potent antagonist ZM241385 were used as controls (Figure 6).

We first tested whether any of the compounds directly induced cAMP production via A_{2A}AR. In contrast to experiments with the known agonist CGS-21680, stimulation of the cells with each of the hit compounds at 10 μM had no effect on cAMP production (Figure 6A), as expected. We next tested whether the hit compounds affected cAMP production in the presence of 1μM CGS21680. ZM241385 served as positive control, showing a full antagonistic effect, as expected (Figure 6B). When tested in the presence of CGS-21680, compounds C1 and C2 showed measurable antagonism of cAMP production at both lower (10 μM) and higher (100 μM) concentrations in a concentration-dependent manner (Figure 6B). Compounds C3 and C4 showed marginal antagonistic

effects at 100 μM concentration and compound C5 showed no measurable impact on cAMP production at either lower or higher concentrations. Based on these results, compounds C1 and C2 were selected for further characterization. Concentration-dependent inhibition of CGS-21680-induced cAMP production was observed for both compounds, with C2 displaying a pIC_{50} of 4.4 and reaching full inhibition at the maximum concentration used, and C1 displaying a pIC_{50} of 5.3 and partial inhibition (Figure 6, C and D). Finally, we tested the activity of the compounds as allosteric modulators by performing concentration-dependent curve of the CGS-21680 agonist in the presence of different concentrations of the compounds. As shown in Figure 6E, compound C2 decreased agonist efficacy in a concentration-dependent manner, reaching full inhibition at 100 μM, without modifying the affinity of the agonist for the receptor (pEC_{50} = 7.9 at 0 μM vs. pEC_{50} = 7.9 at 30 μM). Compound C1 also inhibited CGS-21680-induced cAMP production, reaching full inhibition at 300 μM and, in addition, it decreased the affinity of the agonist for the receptor (pEC_{50} = 7.9 at 0 μM vs. pEC_{50} = 6.9 at 30 μM and 100 μM) (Figure 6F). Altogether, these data provide evidence that compounds C2 and C1 are functionally active on A_{2A}AR and that they behave as negative allosteric modulators (NAMs) of this receptor.

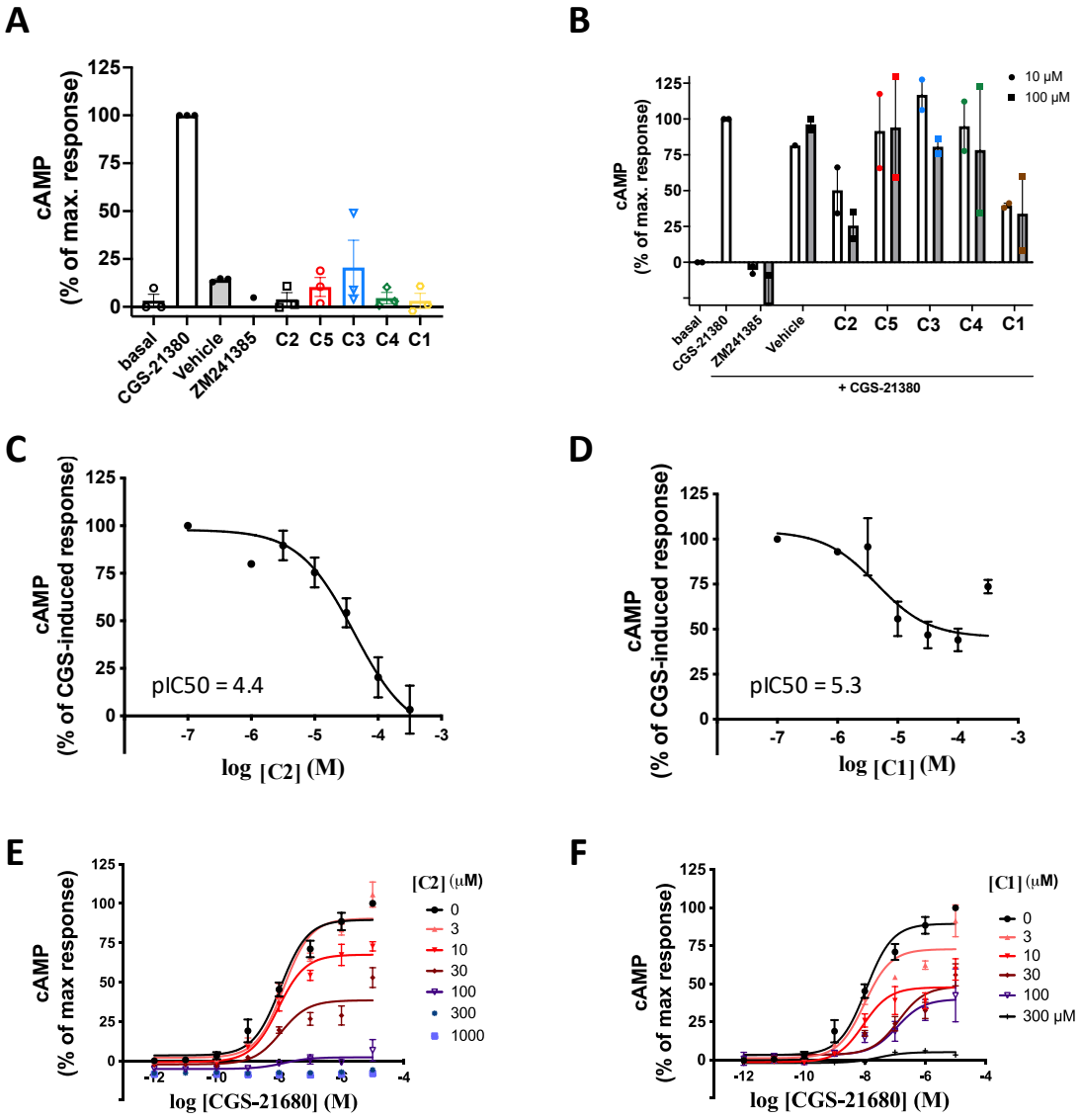

Figure 6. Functional characterization of compounds on the cAMP signaling pathway. A) cAMP production in HEK-A2AR cells stimulated with the reference ligands CGS-21680 (agonist; 1 µM, 30min) and ZM241385 (antagonist, 10 µM, 30min) or with compounds C1 to C5 (10 µM, 30 min). Basal corresponds to non-stimulated cells and vehicle = DMSO 1%. Data are expressed as mean ± S.E.M. of 3 independent experiments and normalized to % of CGS-21680-induced response. **(B)** Analysis of antagonist effect of compounds on CGS-21680-induced cAMP production (1 µM, 30min). Cells were pre-incubated with the reference antagonist (ZM241385, 1 µM) or compounds (10 µM or 100 µM, 15 min) before another 30 min of incubation after adding the agonist CGS-21680. Data are expressed as mean ± S.D. of 2 independent experiments and normalized to % of CGS-21680-induced response. **(C-D)** Concentration-response curves of **(C)** C1 and **(D)** C5 on CGS-21680-induced (1 µM, 30 min) cAMP production. Data are expressed as mean ± S.E.M. of 5 independent experiments and normalized to % of CGS-21680-induced response. **(E-F)** Analysis of allosteric effect of **(E)** C1 and **(F)** C5 by performing the concentration-response curve of the agonist CGS-21680 on cAMP production in the presence of different concentrations of the compounds. Data are expressed as mean ± S.E.M. of 4 independent experiments and normalized to % of CGS-21680-induced response.

Computational modeling of allosteric binding modes

We developed a computational protocol based on tailored analysis of 1 μs-length molecular dynamics (MD) sampling, independently obtained for both the active and inactive conformations of the receptor. The relative configurational entropy is then estimated via mutual information (MI) matrices, which report the degree of correlated movement between residues (Figure 7). We quantify relative configurational entropy via mutual information (MI) matrices, which report the degree of correlated movement between residues (Figure 7). The MI values are converted into MI-intensity histograms that encode the coupling intensity of each residue with amino acids that form the orthosteric binding pocket. The resulting MI intensities can be projected onto the receptor's three-dimensional structure and compared with cavities independently obtained with FTMap, enabling the identification of potential allosteric hotspots. A full description of the procedure is provided in the Supplementary Methods section and illustrated in Figure 7 with results obtained with A_{2A}AR. We initially validated this protocol with the compound MIPS521, a known allosteric modulator of the A_1 adenosine receptor (A_1AR).[23] The protocol correctly identified the allosteric binding site and pose of MIPS521 within this pocket (Figure S1). A manuscript describing thorough benchmarking and validation of this approach is currently in preparation.

Analysis of the MI-intensity histogram in Figure 7 identified strong couplings between several residues known to participate in GPCR signaling and the orthosteric binding site, validating the ability of our approach to detect established allosteric communication pathways in class A GPCRs. These include Trp246$^{6.48}$, the central residue of the CWxP motif associated with the outward movement of TM6 during activation,[20,24-26] and the cluster comprising Gln207$^{5.68}$, Gln210$^{5.71}$, Ile106$^{3.54}$ and Arg291$^{7.56}$, which interacts with the α5 helix of the G_α subunit.[27] Another prominent coupling involves Arg102$^{3.50}$, which, together with Glu228$^{6.30}$, forms the conserved "ionic lock" that favors an inactive conformation. Overlaying regions of high MI coupling with the drug-like cavities identified in the FTMap analysis revealed five potential allosteric hotspot regions in A_{2A}AR (colored regions in Figure 7). Four of these hotspots are located on the intracellular surface of the receptor, designated the ICL2 site, ICL3 site, G-protein binding

site and TM7/TM8 interface, while one site is located on the extracellular surface near the TM7/TM1 interface

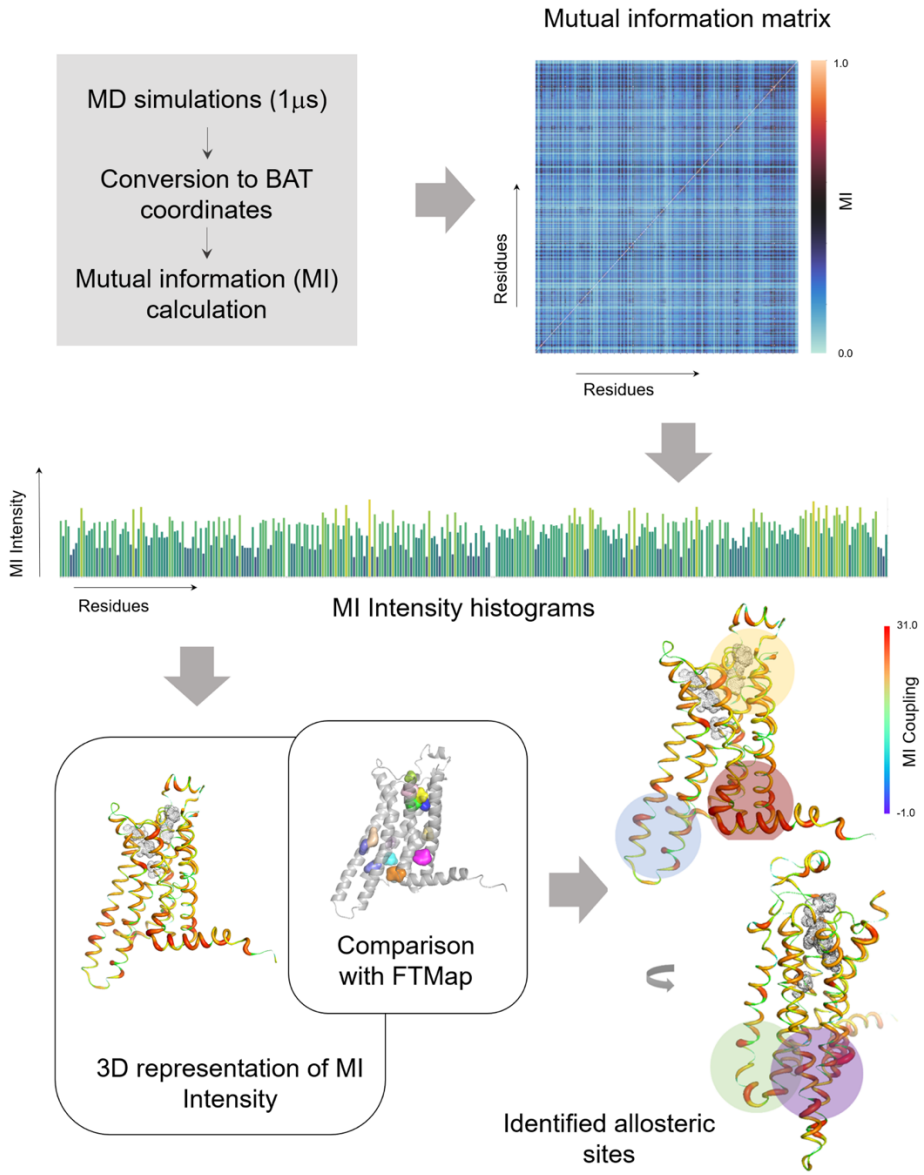

Figure 7. Schematic representation of the computational protocol designed for this study to identify allosteric sites in the A_{2A}AR (see Methods for details). The regions highlighted by colored circles were identified as candidate allosteric binding cavities (see text).

Docking exploration and MD simulations of allosteric molecules C1 and C2

After identifying potential allosteric binding sites (Figure 7), we performed a systematic docking analysis for the two most promising allosteric modulators reported here, C1 and

C2. These molecules contain three (C1) or two (C2) stereocenters with defined relative stereochemistry. However, because of a potential epimerization of the chiral center alpha to the carboxamide moiety, eight stereoisomers were considered in docking for C1. Both enantiomers of C2 were included in the docking analysis. The resulting docking scores are presented as heatmaps based on the top-ranked docking pose, with stereoisomers represented as rows and binding sites as columns (Figures S3 and S4). Molecule C1 shows a clear preference for an extracellular binding site between the extracellular ends of TM1 and TM7 (Figure 7, yellow region), independent of stereochemistry (Figure S3). All eight stereoisomers occupy identical volumes (Figure 8, red ligands). Six stereoisomers adopt an extended orientation in which the biphenyl group points towards the extracellular surface, while the thiophene ring forms a π–π interaction with Phe168^{ECL2} (Figure 8, panel B). The remaining two stereoisomers (R,R,S and R,S,R) adopt a flipped orientation in which the biphenyl and thiophene substituents exchange roles (Figure 8A), suggesting some stereochemical sensitivity that may influence ligand efficacy. This allosteric binding pocket partially overlaps with the orthosteric binding site, as defined in experimental structures of this receptor for both agonist and antagonist complexes,[28] in line with data from the thermal shift assay (Figure 2) and radioligand binding competition assay (Figure 4).

To refine binding site predictions, each docking pose for all eight stereoisomers and across all five candidate binding sites was subjected to MD simulations totaling 12 μs of sampling (triplicate 100 ns trajectories per pose; see Methods). We compared the average number of hydrogen bonds (Figure S6) and average ligand RMSD values (Figure S8) across simulations to evaluate the most probable binding site for each ligand. The number of hydrogen bonds was similar across all poses, with an additional hydrogen bond observed in the G protein binding interface and the extracellular TM1/TM7 interface (Figure S6). Ligand stability was highest in the extracellular site at the TM1/TM7 interface (Figure S8), supporting this region as the most probable binding site for ligand C1. MD simulations revealed that the π–π stacking interaction with Phe168^{ECL2} is complemented by hydrogen bonds between the ligand's amide group and either the backbone carbonyl of Ser67$^{2.68}$ or the sidechain of Tyr271$^{7.36}$ (Figure 8). Interestingly, Tyr271$^{7.36}$ varies among adenosine receptor subtypes and has been implicated in the selectivity of the

partial agonist BAY60-6583 for $A_{2A}AR$, where the acetamide extension of this ligand engages a region not occupied by the endogenous agonist.[29] In the binding mode explored by most stereoisomers, the biphenyl moiety inserts between helices 1 and 7 (Figure 8B), occupying the same region where oleic acid was previously observed,[30] an interaction that is mimicked by the thiophene group in the two stereoisomers that adopt the flipped configuration (Figure 8A). These binding modes provide a mechanistic explanation for the experimentally observed allosteric behavior of ligand C1 (Figure 6F). By occupying a secondary binding pocket, ligand C1 likely stabilizes an inactive receptor conformation, thereby reducing agonist E_{max} while its partial overlap with the orthosteric site may account for the observed rightward shift in EC_{50} (Figure 6F).

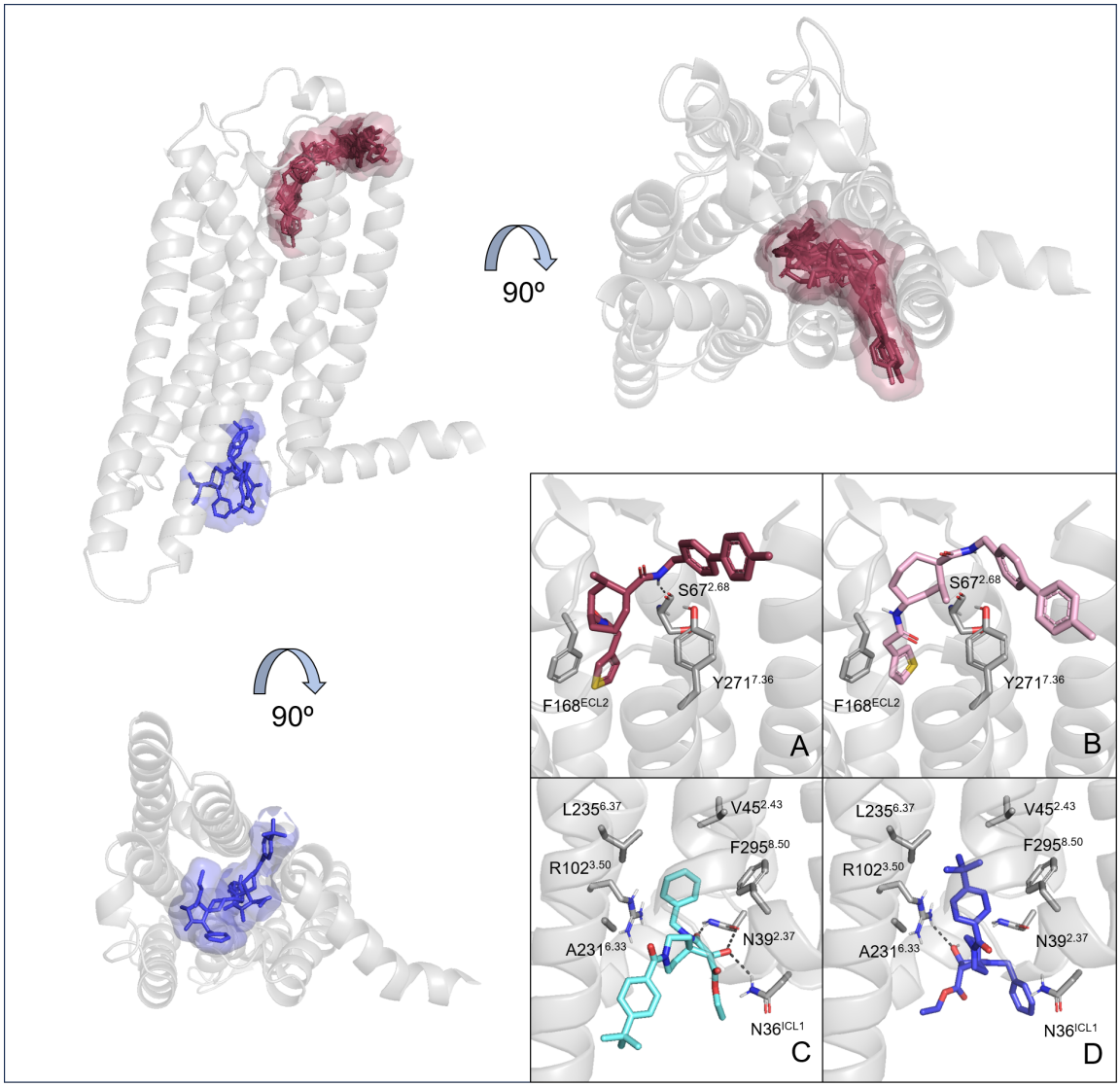

Figure 8. Docking poses selected for the enantiomers of molecule C1 (dark red) and molecule C2 (blue) on the H1/H7 and G protein sites, respectively, of the inactive A_{2A}AR structure. A) side view, parallel to the membrane plane, and orthogonal views from the B) extracellular side and C) intracellular side. An enlarged view of the binding cavities (bottom right) highlights specific interactions in representative docking poses of compound C1 (A: enantiomer EF, B: enantiomer EG) and compound C2 (C: enantiomer AA, D: enantiomer AB).

In the case of compound C2, initial docking studies on both enantiomers did not distinguish among binding sites based on docking scores (Figure S3). However, subsequent MD simulations of the corresponding poses, totaling 3 μs of sampling, revealed a clear preference for the G protein interface, where poses exhibited a higher number of hydrogen bonds and lower average RMSD values compared with other sites. As observed with ligand C1, the two C2 enantiomers adopt distinct binding orientations within the preferred binding site, with exchanged positions of their substituents. The

binding mode of enantiomer $C2_{AA}$ (Figure 8C) is stabilized by hydrogen bonds between the ligand hydroxyl group and Arg102$^{3.50}$, Asn39$^{2.37}$ and Asn35^{ICL1}, while the benzyl substituent fits into a hydrophobic pocket formed by Val45$^{2.43}$, Leu235$^{6.37}$, Phe295$^{8.50}$ and Ala231$^{6.33}$. The second enantiomer, $C2_{AB}$, is anchored instead by a stable hydrogen bond with Arg102$^{3.50}$, which contributes to the formation of an ionic lock in the receptor inactive conformation, while positioning the (*p*)-*t*-but-phenyl group within the same hydrophobic cavity previously occupied by the benzyl moiety (Figure 8D).

The allosteric binding mode proposed for compound C2 is entirely distinct from the orthosteric binding site, consistent with its pharmacological profile (Figure 6E). Specifically, the reduction in agonist E_{max} occurs without a shift in the EC_{50} value, which can be rationalized by the ligand's ability to perturb G-protein signaling without interfering with agonist binding. Indeed, analogous intracellular cavities have been experimentally determined as the binding site of allosteric regulators of several class-A GPCRs, including the β_2-adrenergic receptor, CCR2 and CCR9 chemokine receptors (Figure S2).

DISCUSSION

By leveraging AS-MS with the wild-type, full-length $A_{2A}AR$ and an sp^3-enriched, chemically diverse library, we established a screening strategy that enables discovery of GPCR allosteric modulators without relying on mutations that stabilize specific conformational states. Orthogonal competition and biophysical analyses confirmed the allosteric nature of these compounds. Several hits influenced binding of the antagonist ZM241385, suggesting an interplay between the orthosteric pocket and allosteric sites. All hits exhibited relatively modest to very weak affinities, highlighting the high sensitivity of the AS-MS platform to detect low-affinity, non-orthosteric interactions. Despite their relatively weak affinities, these compounds modulated $A_{2A}AR$ signaling in cAMP accumulation assays. Co-treatment with the $A_{2A}AR$ agonist CGS-21680 classified the ligands as NAMs, and the dependence of their effects on agonist concentration supports a receptor-mediated mechanism rather than nonspecific cellular perturbation. Differences in signaling profiles among the hits suggest mechanistically distinct modes of allosteric regulation.

To gain structural insight into the mechanisms underlying these allosteric effects, we developed a new computational workflow that integrates MD simulations of active and inactive receptor conformations with network analysis and cavity mapping to identify allosteric communication pathways and ligand-accessible binding pockets. This approach enables systematic identification of candidate allosteric sites without requiring prior structural knowledge of ligand binding. While applied here to $A_{2A}AR$, the framework is generalizable across GPCRs, and its broader application to additional receptors and ligands will be reported separately.

Among the candidate allosteric sites, ICL2 has been structurally validated as an allosteric pocket in several other GPCRs, including the dopamine D_1 receptor (D_1R).[31] Modulators binding to this region typically increase the rigidity of ICL2, Modulators binding to this region increase ICL2 rigidity, thereby perturbing the receptor–G protein interface, which is essential for downstream signaling.[32] We propose a similar mechanism for the ICL3 allosteric pocket, given that GPCR activation typically involves coordinated movement of the intracellular end of TM6 and extension of the intracellular end of TM5,[33,34] which are connected by ICL3. Consistent with this, ICL3 loop has been

implicated in β-arrestin recruitment,[35] autoregulation of G-protein signaling,[31] and has been proposed to be an allosteric binding site.[36]

Allosteric regulation mediated through the G protein binding site identified in our analysis (Figure 7, purple region) is most likely competitive, in line with analogous sites identified in β_2AR[36], CCR9[37] and CCR2.[38] Adjacent to this site, a hotspot at the TM7–H8 interface contains the highly conserved NPxxY motif, which plays central roles in receptor activation, biased signaling, receptor internalization, and β-arrestin engagement.[39] Modulation of conformational plasticity at this site therefore represents a plausible mechanism for allosteric regulation, as supported by prior studies demonstrating that small molecule NAMs interacting with this region in the CCR2 chemokine receptor can alter orthosteric ligand binding.[38,40] Finally, the extracellular pocket located at the interface between TM1 and TM7 (Figure 7, yellow region) has been identified as an allosteric site in several GPCRs including muscarinic acetylcholine receptors (mAChR)[41]. Proposed mechanisms of allosteric modulation range from direct competitive binding to stabilization of specific active or inactive receptor conformational states.

In summary, this work demonstrates that allosteric NAMs targeting A_{2A}AR can operate through multiple, structurally distinct mechanisms, highlighting the richness and diversity of the allosteric landscape in this therapeutically important receptor. Allosteric modulation of A_{2A}AR is an emerging strategy for therapeutic intervention, yet the repertoire of known allosteric ligands remains limited and generally less selective than orthosteric agents. This disparity reflects intrinsic challenges in allosteric ligand discovery, including transient or cryptic binding sites, lower intrinsic druggability, and the lack of screening platforms capable of detecting weak, non-orthosteric interactions. The integrated experimental and computational approach presented here addresses several of these challenges and provides a broadly applicable framework for discovering GPCR allosteric modulators, as well as tractable starting points for the development of optimized therapeutic leads.

ASSOCIATED CONTENT

The Supporting Information contains experimental details, including sample preparation protocols, details on the experimental methods, and details on the computational methods. The Supporting Information also contains Tables S1-S4, related to the fluorescence thermal shift and radioligand binding experiments, and Figures S1 through S8, related to the computational work in this study.

AUTHOR INFORMATION

AW, RP : AS-MS screening

HL, DR : Compounds and library design

EF, SN : compounds synthesis

AM, MD, SI, AJ, RS, KK : protein production and QC

NT, AR, ME : Biophysical characterization of hits

TT, HG : computational modeling

EC, RJ : cAMP signaling assays

DR, ME, RJ, HG, RP : Project management and supervision

DR, HL, ME, RJ, EC, HG, TT, RP : Writing, reviewing and editing with input from all

ACKNOWLEDGEMENTS

N.T., A.P.R., and M.T.E. were supported by an NIH MIRA award R35GM138291.

This work was supported by the Fondation pour la Recherche Médicale (Equipe FRM EQU202503020060, to R.J.), This work was supported by the Agence Nationale de la Recherche (ANR- 23-CE18-0008 SENS-AD, to E.C.), the Fondation de la Recherche Médicale (MND202310017920, to E.C.), "Projet de recherche international" (PRI) Inserm édition 2023, Institut National de la Santé et de la Recherche Médicale (INSERM) and Centre National de la Recherche Scientifique (CNRS). This study was supported by grant PID2023-150793OB-I00 from the Spanish Ministry of Science and Innovation. Computations were enabled by resources provided by the National Academic Infrastructure for Supercomputing in Sweden (NAISS) and the Swedish National Infrastructure for Computing (SNIC) partially funded by the Swedish Research Council through grant agreements no. 2022-06725 and no. 2018-05973.

COMPETING INTERESTS

HL, DR and RP are employees and shareholders of Edelris SA.

Other authors declare no competing interests.

ABBREVIATIONS

$A_{2A}AR$	: A_{2A} Adenosine Receptor
ALIS	: Automated Ligand Identification System
AS-MS	: Affinity Selection Mass Spectrometry
BR	: Binding Ratio
cAMP	: cyclic Adenosine MonoPhosphate
GPCR	: G Protein Coupled Receptor
HMA	: HexaMethylene Amiloride
HRMS	: High Resolution Mass Spectrometry
HTRF	: Homogeneous Time Revolved Fluorescence
ICL	: Intracellular loop
IC_{50}	: Inhibitory Concentration 50%
MST	: MicroScale Thermophoresis
MI	: Mutual information
MIST	: Mutual Information Spanning Tree
NAM	: Negative Allosteric Modulator
PD-1/PD-L1	: Programmed cell Death protein 1 / PD Ligand 1
QC	: Quality Control
LC	: Liquid Chromatography
RMSD	: Root Mean Square Deviation
SEC	: Size Exclusion Chromatography
s.e.m	: Standard Error Mean
Tm	: Melting Temperature
TM	: Transmembrane

REFERENCES

(1) Deb, P. K.; Maity, P.; Sarkar, B.; Venugopala, K. N.; Tekade, R. K.; Batra, S. Insights from Clinical Trials on A2A Adenosine Receptor Antagonists for Cancer Treatment. *ACS Pharmacology & Translational Science* **2025**, *8* (6), 1498-1512.

(2) Beavis, P. A.; Milenkovski, N.; Henderson, M. A.; John, L. B.; Allard, B.; Loi, S.; Kershaw, M. H.; Stagg, J.; Darcy, P. K. Adenosine receptor 2A blockade increases the efficacy of anti–PD-1 through enhanced antitumor T-cell responses. *Cancer immunology research* **2015**, *3* (5), 506-517.

(3) Lei, Q.; Wang, D.; Sun, K.; Wang, L.; Zhang, Y. Resistance mechanisms of anti-PD1/PDL1 therapy in solid tumors. *Frontiers in cell and developmental biology* **2020**, *8*, 672.

(4) Roh, M.; Wainwright, D. A.; Wu, J. D.; Wan, Y.; Zhang, B. Targeting CD73 to augment cancer immunotherapy. *Curr. Opin. Pharmacol.* **2020**, *53*, 66-76.

(5) Young, A.; Ngiow, S. F.; Barkauskas, D. S.; Sult, E.; Hay, C.; Blake, S. J.; Huang, Q.; Liu, J.; Takeda, K.; Teng, M. W. Co-inhibition of CD73 and A2AR adenosine signaling improves anti-tumor immune responses. *Cancer Cell* **2016**, *30* (3), 391-403.

(6) Willingham, S. B.; Ho, P. Y.; Hotson, A.; Hill, C.; Piccione, E. C.; Hsieh, J.; Liu, L.; Buggy, J. J.; McCaffery, I.; Miller, R. A. A2AR antagonism with CPI-444 induces antitumor responses and augments efficacy to anti–PD-(L) 1 and anti–CTLA-4 in preclinical models. *Cancer immunology research* **2018**, *6* (10), 1136-1149.

(7) Qin, S.; Meng, M.; Yang, D.; Bai, W.; Lu, Y.; Peng, Y.; Song, G.; Wu, Y.; Zhou, Q.; Zhao, S. High-throughput identification of G protein-coupled receptor modulators through affinity mass spectrometry screening. *Chemical science* **2018**, *9* (12), 3192-3199.

(8) Gutiérrez-de-Terán, H.; Massink, A.; Rodríguez, D.; Liu, W.; Han, G. W.; Joseph, J. S.; Katritch, I.; Heitman, L. H.; Xia, L.; IJzerman, A. P. The role of a sodium ion binding site in the allosteric modulation of the A2A adenosine G protein-coupled receptor. *Structure* **2013**, *21* (12), 2175-2185.

(9) Prudent, R.; Annis, D. A.; Dandliker, P. J.; Ortholand, J.-Y.; Roche, D. Exploring new targets and chemical space with affinity selection-mass spectrometry. *Nature Reviews Chemistry* **2021**, *5* (1), 62-71.

(10) Igonet, S.; Raingeval, C.; Cecon, E.; Pučić-Baković, M.; Lauc, G.; Cala, O.; Baranowski, M.; Perez, J.; Jockers, R.; Krimm, I. Enabling STD-NMR fragment screening using stabilized native GPCR: A case study of adenosine receptor. *Sci. Rep.* **2018**, *8* (1), 8142.

(11) Conflitti, P.; Lyman, E.; Sansom, M. S.; Hildebrand, P. W.; Gutiérrez-de-Terán, H.; Carloni, P.; Ansell, T. B.; Yuan, S.; Barth, P.; Robinson, A. S. Functional dynamics of G

protein-coupled receptors reveal new routes for drug discovery. *Nat. Rev. Drug Disc.* **2025**, *24* (4), 251-275.

(12) Guo, J.; Zhou, H.-X. Protein allostery and conformational dynamics. *Chem. Rev.* **2016**, *116* (11), 6503-6515.

(13) Tzeng, S.-R.; Kalodimos, C. G. Protein activity regulation by conformational entropy. *Nature* **2012**, *488* (7410), 236-240.

(14) Corvest, V.; Jawhari, A. Solubilization and stabilization of native membrane proteins for drug discovery. In *Multiprotein Complexes: Methods and Protocols*, Springer, 2020; pp 257-267.

(15) Annis, A.; Chuang, C. C.; Nazef, N. ALIS: an affinity selection–mass spectrometry system for the discovery and characterization of protein–ligand interactions. *Mass spectrometry in medicinal chemistry: applications in drug discovery* **2007**, 121-156.

(16) Muckenschnabel, I.; Falchetto, R.; Mayr, L.; Filipuzzi, I. SpeedScreen: label-free liquid chromatography–mass spectrometry-based high-throughput screening for the discovery of orphan protein ligands. *Anal. Biochem.* **2004**, *324* (2), 241-249.

(17) Irwin, J. J.; Duan, D.; Torosyan, H.; Doak, A. K.; Ziebart, K. T.; Sterling, T.; Tumanian, G.; Shoichet, B. K. An aggregation advisor for ligand discovery. *J. Med. Chem.* **2015**, *58* (17), 7076-7087.

(18) Alexandrov, A. I.; Mileni, M.; Chien, E. Y. T.; Hanson, M. A.; Stevens, R. C. Microscale fluorescent thermal stability assay for membrane proteins. *Structure* **2008**, *16* (3), 351-359.

(19) Thakur, N.; Wei, S.; Ray, A. P.; Lamichhane, R.; Eddy, M. T. Production of human A2AAR in lipid nanodiscs for 19F-NMR and single-molecule fluorescence spectroscopy. *STAR Protocols* **2022**, *3* (3), 101535.

(20) Eddy, M. T.; Lee, M.-Y.; Gao, Z.-G.; White, K. L.; Didenko, T.; Horst, R.; Audet, M.; Stanczak, P.; McClary, K. M.; Han, G. W.; et al. Allosteric coupling of drug binding and intracellular signaling in the A2A adenosine receptor. *Cell* **2018**, *172* (1-2), 68-80.

(21) Jaakola, V.-P.; Griffith, M. T.; Hanson, M. A.; Cherezov, V.; Chien, E. Y. T.; Lane, J. R.; IJzerman, A. P.; Stevens, R. C. The 2.6 angstrom crystal structure of a human A_{2A} adenosine receptor bound to an antagonist. *Science* **2008**, *322* (5905), 1211-1217.

(22) Gao, Z.-G.; Ijzerman, A. P. Allosteric modulation of A2A adenosine receptors by amiloride analogues and sodium ions. *Biochem. Pharmacol.* **2000**, *60* (5), 669-676.

(23) Draper-Joyce, C. J.; Bhola, R.; Wang, J.; Bhattarai, A.; Nguyen, A. T.; Cowie-Kent, I.; O'Sullivan, K.; Chia, L. Y.; Venugopal, H.; Valant, C. Positive allosteric mechanisms of adenosine A1 receptor-mediated analgesia. *Nature* **2021**, *597* (7877), 571-576.

(24) Wei, S.; Pour, N. G.; Tiruvadi-Krishnan, S.; Ray, A. P.; Thakur, N.; Eddy, M. T.; Lamichhane, R. Single-molecule visualization of human A2A adenosine receptor activation by a G protein and constitutively activating mutations. *Communications Biology* **2023**, *6* (1), 1218.

(25) Ma, N.; Lee, S.; Vaidehi, N. Activation microswitches in adenosine receptor A2A function as rheostats in the cell membrane. *Biochemistry* **2020**, *59* (42), 4059-4071.

(26) Pellissier, L. P.; Sallander, J.; Campillo, M.; Gaven, F.; Queffeulou, E.; Pillot, M.; Dumuis, A.; Claeysen, S.; Bockaert, J.; Pardo, L. Conformational toggle switches implicated in basal constitutive and agonist-induced activated states of 5-hydroxytryptamine-4 receptors. *Mol. Pharmacol.* **2009**, *75* (4), 982-990.

(27) Carpenter, B.; Nehmé, R.; Warne, T.; Leslie, A. G. W.; Tate, C. G. Structure of the adenosine A2A receptor bound to an engineered G protein. *Nature* **2016**, *536* (7614), 104-107.

(28) Xu, F.; Wu, H.; Katritch, V.; Han, G. W.; Jacobson, K. A.; Gao, Z.-G.; Cherezov, V.; Stevens, R. C. Structure of an Agonist-Bound Human A2A Adenosine Receptor. **2011**, *332*.

(29) Tandaric, T.; Gutiérrez-de-Terán, H. Ligand and residue free energy perturbations solve the dual binding mode proposal for an A2BAR partial agonist. *The Journal of Physical Chemistry B* **2025**, *129* (3), 886-899.

(30) Liu, W.; Chun, E.; Thompson, A. A.; Chubukov, P.; Xu, F.; Katritch, V.; Han, G. W.; Roth, C. B.; Heitman, L. H.; IJzerman, A. P.; et al. Structural Basis for Allosteric Regulation of GPCRs by Sodium Ions. *Science* **2012**, *337* (6091), 232-236.

(31) Wang, X.; Hembre, E. J.; Goldsmith, P. J.; Beck, J. P.; Svensson, K. A.; Willard, F. S.; Bruns, R. F. Mutual cooperativity of three allosteric sites on the dopamine D1 receptor. *Mol. Pharmacol.* **2023**, *103* (3), 176-187.

(32) Zhuang, Y.; Krumm, B.; Zhang, H.; Zhou, X. E.; Wang, Y.; Huang, X.-P.; Liu, Y.; Cheng, X.; Jiang, Y.; Jiang, H. Mechanism of dopamine binding and allosteric modulation of the human D1 dopamine receptor. *Cell Res.* **2021**, *31* (5), 593-596.

(33) Carpenter, B.; Tate, C. G. Engineering a minimal G protein to facilitate crystallisation of G protein-coupled receptors in their active conformation. *Protein Eng. Des. Sel.* **2016**, *29*, 583-594.

(34) García-Nafría, J.; Lee, Y.; Bai, X.; Carpenter, B.; Tate, C. G. Cryo-EM structure of the adenosine A2A receptor coupled to an engineered heterotrimeric G protein. *eLife* **2018**, *7*.

(35) Ferguson, S. S.; Downey III, W. E.; Colapietro, A.-M.; Barak, L. S.; Ménard, L.; Caron, M. G. Role of β-arrestin in mediating agonist-promoted G protein-coupled receptor internalization. *Science* **1996**, *271* (5247), 363-366.

(36) Liu, X.; Ahn, S.; Kahsai, A. W.; Meng, K.-C.; Latorraca, N. R.; Pani, B.; Venkatakrishnan, A.; Masoudi, A.; Weis, W. I.; Dror, R. O. Mechanism of intracellular allosteric β2AR antagonist revealed by X-ray crystal structure. *Nature* **2017**, *548* (7668), 480-484.

(37) Oswald, C.; Rappas, M.; Kean, J.; Doré, A. S.; Errey, J. C.; Bennett, K.; Deflorian, F.; Christopher, J. A.; Jazayeri, A.; Mason, J. S. Intracellular allosteric antagonism of the CCR9 receptor. *Nature* **2016**, *540* (7633), 462-465.

(38) Zheng, Y.; Qin, L.; Zacarías, N. V. O.; de Vries, H.; Han, G. W.; Gustavsson, M.; Dabros, M.; Zhao, C.; Cherney, R. J.; Carter, P. Structure of CC chemokine receptor 2 with orthosteric and allosteric antagonists. *Nature* **2016**, *540* (7633), 458-461.

(39) Schönegge, A.-M.; Gallion, J.; Picard, L.-P.; Wilkins, A. D.; Le Gouill, C.; Audet, M.; Stallaert, W.; Lohse, M. J.; Kimmel, M.; Lichtarge, O. Evolutionary action and structural basis of the allosteric switch controlling β2AR functional selectivity. *Nat. Comm.* **2017**, *8* (1), 2169.

(40) Zweemer, A. J.; Nederpelt, I.; Vrieling, H.; Hafith, S.; Doornbos, M. L.; de Vries, H.; Abt, J.; Gross, R.; Stamos, D.; Saunders, J. Multiple binding sites for small-molecule antagonists at the CC chemokine receptor 2. *Mol. Pharmacol.* **2013**, *84* (4), 551-561.

(41) Ferruz, N.; Doerr, S.; Vanase-Frawley, M. A.; Zou, Y.; Chen, X.; Marr, E. S.; Nelson, R. T.; Kormos, B. L.; Wager, T. T.; Hou, X. Dopamine D3 receptor antagonist reveals a cryptic pocket in aminergic GPCRs. *Sci. Rep.* **2018**, *8* (1), 897.